2-D numerical modelling of magnetotelluric fields in anisotropic structures - an FD algorithm

Josef Pek

Geophys. Inst., Acad. Sci. Czech Rep., Prague, Czech Republic

Abstract

An algorithm for numerical modelling of magnetotelluric fields in 2-D anisotropic block structures is proposed. Electrical properties of the individual homogeneous blocks are given by an arbitrary symmetric and positive definite conductivity tensor. The problem leads to a coupled system of differential equations for the strike-parallel components of the magnetotelluric field, E_x and H_x. These equations are approximated by the finite difference method, using the integration approach. Use is made of the constancy of the magnetic H_x component in the non-conductive air so that only equations for the electric mode are approximated within the air layer. The system of linear difference equations, resulting from the FD approximation, can be arranged in such a way that its matrix is symmetric and band-limited, and can be solved, for not too large models, by Gaussian elimination. The algorithm is applied to model situations which demonstrate the effect of 2-D anisotropy on the relation between magnetotelluric impedances and induction arrows.

1 Motivation

Recently several attempts to interpret magnetotelluric data have appeared in which strong electrical anisotropy of deep geoelectrical structures played a substantial role, 'strong' meaning as much as several orders of magnitude in terms of the anisotropy ratio $\lambda = \rho_{max}/\rho_{min}$. To mention at random, e.g. Tezkan [1] presented a model for magnetotelluric data from the eastern margin of the Hessische Senke (Germany) in which a crustal pseudo-anisotropic conductor (vertical dykes with conductivity contrast of 100 Ωm/5 Ωm) was introduced below the transition from the Rhenohercynicum to the northern Phyllite Zone to account for the systematic divergence of magnetotelluric E and H polarization phases towards long periods. In [2] another example of a similar interpretation is presented for induction data from the contact zone between the Rhine Graben and Black Forest (Germany) where a deep anisotropic layer (dyke conductivity contrast of almost 10^3) is assumed at the depth of about 12 km under the Black Forest stations to explain both the magnetotelluric phases and induction vectors in this region.

Similarly, a strongly anisotropic structure of regional extent (λ as much as 10^3!) is proposed by several authors (e.g. [3, 4, 5]) to explain strong anisotropy of the magnetotelluric curves and a systematic discrepancy between the magnetotelluric impedances and induction arrows in a broader vicinity of the ultradeep drilling site KTB in Oberpfalz (Germany). As a physical source of this strong anisotropy a joint effect of narrow, nearly vertical, graphitized cataclastic zones, detected in this region in near surface structures, is hypothesized [3], although other physical mechanisms cannot be excluded either [4].

Interpreting the BC87 data set from British Columbia (Canada) Eisel and Bahr [7] and Jones et al. [8] both arrive at the conclusion that a strongly anisotropic layer (λ as much as 10^2) at lower crust/upper mantle depths is required for their models to fit the magnetotelluric data at longer periods. A similar phenomenon, with the anisotropic structure situated in the lower crust, is discussed by Rasmussen [9] with regard to his magnetotelluric data from Sweden.

At present the most challenging, but also the most difficult problem is undoubtedly the question of what the physical mechanisms can be which generate, or simulate, such strong anisotropies within the deep structures of the earth. Unfortunately, we totally ignore this principal question in this contribution, and turn our attention to a much simpler problem of analyzing the influence of anisotropic domains upon the electromagnetic data in case of laterally inhomogeneous, particularly 2-D geoelectrical structures.

Methods currently used for modelling the effects of electrical anisotropy on the magnetotelluric data are mostly based on rather oversimplified assumptions—either 1-D approximations of the earth's structure are employed on local scale, or 2-D models are used with different conductivities for the E and

H polarization mode respectively, constraining thus the anisotropy in such a way that the conductivity tensor must reduce to the diagonal form just in the strike-bound coordinate system. A physically more plausible model of the electrical anisotropy, used in a series of interpretations (e.g. [1, 3]), and based on stacking alternately conductive and nonconductive dykes, is subject to the same constraint. Except one can make use of powerful 3-D modelling tools, only structures with dykes parallel to the model's strike can be managed. It is clear that particularly the above 2-D approximations of the electrical anisotropy do remain within the scope of 2-D algorithms currently used to model isotropic geoelectrical structures, and they do not allow a lot of features, which are intuitively expected to be generated by anisotropic subdomains within the structure, to be revealed and analyzed.

Although a sufficiently general finite element algorithm for modelling magnetotelluric fields in 2-D structures with authentic anisotropy was already published now nearly twenty years ago [10], it has not been made use of in practical applications yet, as far as we know. Since then, articles dealing with anisotropy in multidimensional geoelectrical structures have appeared only sporadically, e.g. [11, 12, 13]. Now, obviously under the influence of the very practical problems like those mentioned for illustration above, this question seems to draw more attention again, as may be also evidenced by a few more papers presented at this colloquy [14, 15]

The main aim of this contribution is to present a new version of a numerical algorithm which makes it possible to model magnetotelluric fields in 2-D structures containing quite generally anisotropic subdomains. Since much of the general ideas of the method is adopted from [10] we do not pretend to have developed a new algorithm, we rather consider our version a 'come back' of an old method with a few new features, from which the following ones are worth mentioning: (i) the physical problem is approximated by the method of finite differences, (ii) the conductivity tensor within each of the anisotropic subdomains of the medium can be represented by an arbitrary symmetric, positive definite matrix, allowing thus both horizontal and dipping anisotropies to be modelled, and (iii) for the quasi-stationary case, the numerical approximation of the H-mode equations is avoided within the non-conductive air layer.

2 Mathematical formulation of the problem

We assume a traditional 2-D geoelectric model with the structural strike parallel to the x-axis of the Cartesian coordinate system. The z-axis is positive downward. The model consists of a finite system of homogeneous, but in general anisotropic 2-D blocks. 2-D inhomogeneities are restricted to a finite region. Outside this region the structure merges into its anisotropic layered background, which can be in general different for either side of the model. The earth's surface is supposed to be planar (no topography is considered in this model) and to coincide with the coordinate plane $z = 0$. Above the surface a perfectly insulating air layer is assumed. The primary electromagnetic field is modeled as a monochromatic electromagnetic plane wave (angular frequency $\omega = 2\pi/T$, with T being the period) impeding perpendicularly to the earth's surface from sources located at $z = -\infty$.

In the quasi-steady state approximation the governing equations for the electromagnetic field in each of the homogeneous subregions of the model are Maxwell's equations

$$\nabla \times \vec{E} = i\omega\mu_0\vec{H}, \qquad \nabla \times \vec{H} = \hat{\sigma}\vec{E} \tag{1}$$

where a time factor $e^{-i\omega t}$ is assumed. By virtue of the symmetry condition $\partial/\partial x = 0$, these equations, written for the x, y, and z-coordinates, reduce to

$$\frac{\partial E_z}{\partial y} - \frac{\partial E_y}{\partial z} = i\omega\mu_0 H_x, \tag{2}$$

$$\frac{\partial E_x}{\partial z} = i\omega\mu_0 H_y, \tag{3}$$

$$-\frac{\partial E_x}{\partial y} = i\omega\mu_0 H_z, \tag{4}$$

$$\frac{\partial H_z}{\partial y} - \frac{\partial H_y}{\partial z} = \sigma_{xx}E_x + \sigma_{xy}E_y + \sigma_{xz}E_z, \tag{5}$$

$$\frac{\partial H_x}{\partial z} = \sigma_{yx}E_x + \sigma_{yy}E_y + \sigma_{yz}E_z, \tag{6}$$

$$-\frac{\partial H_x}{\partial y} = \sigma_{zx}E_x + \sigma_{zy}E_y + \sigma_{zz}E_z, \tag{7}$$

We will suppose throughout this paper that the conductivity tensor $\hat{\sigma}$ is symmetric and positive definite. In practical implementation within our computer program the conductivity tensor is defined by its three principal values and by three rotation angles, analogous to Euler's elementary rotations known from classical mechanics. The conductivity tensor is constructed by applying to its diagonal, principal form successively three rotations—first around z-axis by the anisotropy strike angle, then around the new x-axis by the anisotropy dip angle, and finally around the current z-axis by the third angle involved. In such a way any orientation of the principal axes of the conductivity tensor in space can be achieved.

To complete the mathematical formulation of the problem we must add the boundary conditions for the field components, both on inner and outer boundaries of the model. On inner boundaries, where blocks of different electrical properties make contact, the following conditions must hold: (i) continuity of the tangential component of the electric field $\vec{E}$, (ii) continuity of the normal component of the current density $\vec{j} = \hat{\sigma}\vec{E}$, and (iii) continuity of all the components of the magnetic field $\vec{H}$, as we suppose the magnetic permeability to be equal to its vacuum value, $\mu = \mu_0 = 4\pi \times 10^{-7}$ H/m, everywhere within the model.

On the outer boundaries of the model Dirichlet boundary conditions are set, constructed from 1-D solutions for the corresponding layered media at the left and right hand side of the model. In our version of the computer program this is accomplished by applying a matrix propagation method to the vector composed of the horizontal components of the magnetotelluric field. This procedure may be considered a slight modification of well-known techniques of [16] or [17].

From equations (2) through (7), the field components E_y, E_z, H_y, and H_z can be eliminated, which, after some algebra, yields a *coupled* pair of second-order partial differential equations for E_x and H_x,

$$\frac{\partial^2 E_x}{\partial y^2} + \frac{\partial^2 E_x}{\partial z^2} + i\omega\mu_0 \left(\sigma_{xx} + A\sigma_{zx} + B\sigma_{yx}\right) E_x + \\ + i\omega\mu_0 A \frac{\partial H_x}{\partial y} + i\omega\mu_0 B \frac{\partial H_x}{\partial z} = 0 \tag{8}$$

for the E-mode, where

$$A = (\sigma_{xy}\sigma_{yz} - \sigma_{xz}\sigma_{yy})/D, \qquad B = (\sigma_{xz}\sigma_{zy} - \sigma_{xy}\sigma_{zz})/D,$$
$$D = \sigma_{yy}\sigma_{zz} - \sigma_{zy}\sigma_{yz},$$

and, for the H-mode,

$$\frac{\partial}{\partial y}\left(\frac{\sigma_{yy}}{D}\frac{\partial H_x}{\partial y}\right) + \frac{\partial}{\partial z}\left(\frac{\sigma_{zz}}{D}\frac{\partial H_x}{\partial z}\right) + \frac{\partial}{\partial y}\left(\frac{\sigma_{zy}}{D}\frac{\partial H_x}{\partial z}\right) + \frac{\partial}{\partial z}\left(\frac{\sigma_{yz}}{D}\frac{\partial H_x}{\partial y}\right) + \\ + i\omega\mu_0 H_x - \frac{\partial(LE_x)}{\partial y} + \frac{\partial(KE_x)}{\partial z} = 0, \tag{9}$$

where

$$K = (\sigma_{zy}\sigma_{yx} - \sigma_{yy}\sigma_{zx})/D, \qquad L = (\sigma_{yz}\sigma_{zx} - \sigma_{zz}\sigma_{yx})/D,$$
$$D = \sigma_{yy}\sigma_{zz} - \sigma_{zy}\sigma_{yz}.$$

It can be seen immediately that for a symmetric conductivity tensor the following identity relations between the coefficients of equations (8) and (9) hold true

$$A = L, \qquad B = K. \tag{10}$$

Of course, there is not a 'pure' E-mode or H-mode any more in generally anisotropic media. The coupling between the modes is expressed through the first-order terms in equations (8) and (9). For these terms to vanish the conductivity tensor must be of degenerate form with $\sigma_{xz} = \sigma_{xy} = 0$, i.e. the coupling between the field modes dissolves if the anisotropy strike is zero. Then equations (8) and (9) decouple into two separate, 'pure' field modes. The conductivity tensor then reduces to $\hat{\sigma} = \begin{pmatrix} \sigma_{xx} & \vec{0} \\ \vec{0}^T & \hat{\sigma}^H \end{pmatrix}$, where $\vec{0}$ is for zero-vector, and $\hat{\sigma}^H = \begin{pmatrix} \sigma_{yy} & \sigma_{yz} \\ \sigma_{zy} & \sigma_{zz} \end{pmatrix}$ describes the anisotropy which affects solely the H-mode solution. Non-zero values of the non-diagonal elements of $\hat{\sigma}^H$ cause the mixed-derivatives terms to appear in (9).

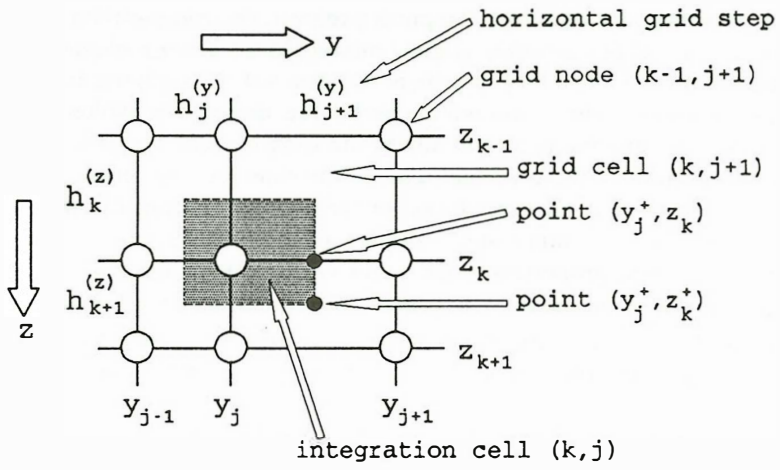

Figure 1: Section of the FD grid around the node point (j,k) along with geometrical grid parameters explained.

3 Numerical approximation

To approximate numerically the governing equations (8) and (9) we will use the finite-differences (FD) method in a most traditional way as it was used earlier to model 2-D isotropic structures (e.g. [18, 19, 20]). First of all, the structure is projected onto a numerical grid and, within a finite grid region, subdivided into a system of electrically homogeneous, but in general anisotropic rectangular grid cells. The grid is in general irregular and it is supposed both to fit the geometry of the model and to meet general rules accepted for designing numerical grids in induction modelling studies for isotropic structures (e.g. [21]), respecting, however, the fact that, unlike scalar conductivities in isotropic structures, the tensorial conductivities are characterized by a range of values rather than by a single value.

Following [20], we use the integration method to derive the FD equations at individual grid nodes. In this approach equations (8) and (9) are integrated across a rectangular integration cell, say, $[y_j - \frac{1}{2}h_j^{(y)}, y_j + \frac{1}{2}h_{j+1}^{(y)}] \times [z_k - \frac{1}{2}h_k^{(z)}, z_k + \frac{1}{2}h_{k+1}^{(z)}] = [y_j^-, y_j^+] \times [z_k^-, z_k^+]$, if node (j,k) is considered (Fig.1), and only these integrals are approximated around the grid point involved. Thus, the integral rather than the differential form of the basic field equations (8) and (9) is used for the FD approximation.

Although a bit tedious, the integration is quite a straightforward procedure and will not be given here in detail. As far as possible the integration is carried out exactly. Several steps, however, involve approximations of the field values and their derivatives. The following four formulae summarize the nature of all the approximation steps employed in the course of evaluating the integrals:

$$\frac{\partial F(y_j^+, z)}{\partial y} \simeq \frac{F(j+1,k) - F(j,k)}{h_{j+1}^{(y)}} \quad \text{for } z \in [z_k^-, z_k^+],$$

$$F(y,z) \simeq F(j,k) \quad \text{for } z \in [y_j^-, y_j^+] \times [z_k^-, z_k^+],$$

$$F(y_j^+, z_k) \simeq \frac{1}{2}[F(j,k) + F(j+1,k)],$$

$$F(y_j^+, z_k^+) \simeq \frac{1}{4}[F(j,k) + F(j+1,k) + F(j,k+1) + F(j+1,k+1)],$$

These formulae refer to particular points marked in Fig.1 and must be altered appropriately if different points are considered.

For an arbitrary grid point (j,k) the FD approximation results in a pair of linear algebraic equations

$$\sum_{p=j-1}^{j+1} \sum_{q=k-1}^{k+1} C_{jk}^{ME}(p,q)\, E_x(p,q) + \sum_{p=j-1}^{j+1} \sum_{q=k-1}^{k+1} C_{jk}^{MH}(p,q)\, H_x(p,q) = 0, \quad M = E, H, \qquad (11)$$

which relate the components E_x and H_x at the central node (j,k) to their eight nearest neighbours in the grid. Falls a grid point involved in equations (11) on the outer boundary of the grid region, then the field values at this node are replaced by the appropriate boundary conditions and the corresponding terms are transferred to the right-hand sides of equations (11).

In Appendix to this article all the coefficients $C_{jk}^{MN}(p,q)$, $M = E,H$, $N = E,H$, $p = j-1, j, j+1$, $q = k-1, k, k+1$ are given explicitely. From these FD scheme patterns we can see that the matrix of coefficients $C_{jk}^{MN}(p,q)$ is never fully occupied, i.e. we need not deal with a 9-point, i.e. 18-value scheme in any case. For the E-mode, we have a 5-point (10-value) scheme only. For the H-mode a complete 9-point scheme must be considered, it contains, however, 14 non-zero coefficients only. These are maximum numbers of coefficients, with full anisotropy considered. The number of coefficients will decrease as the anisotropy within the involved grid cells degenerates.

The FD scheme particularly simplifies within the insulating air layer. By virtue of equations (6) and (7), $\partial H_x/\partial z = 0$ and $\partial H_x/\partial y = 0$ in the air, i.e. H_x is constant everywhere in the air, and equation (9) need not be approximated at all. Equation (8) reduces to Laplace equation. Hence, within the air layer only the E-mode equation is FD approximated, which yields a 5-point FD scheme with only 5 coefficients C_{jk}^{EE}.

4 Solution of the FD equations

Having the governing field equations (8) and (9) FD approximated at all grid nodes, the linear algebraic equations (11) must be properly arranged into a system for further treatment. This may seem a bit intricate task since two sets of variables are involved, E_x and H_x. Moreover, these variables are not sought on identical sets of grid nodes—while the E-mode equation is approximated throughout the grid, the H-mode equation is to be solved within the conducting earth only.

Two possibilities of arranging the variables into an array are obvious (Fig. 2). For both, the variables are ordered throughout the grid in a column-by-column manner, but row-by-row alternative is possible as well. In the first variant, (i), at first all electric components are ordered throughout the grid, from the top to the bottom within each column, and afterwards a block of magnetic components, ordered in the very same way, is joined to the electric array (Fig. 2, left). In the second variant, (ii), within a column, electric components are ordered in succession from the top of the column to the earth's surface, and then, inside the earth, electric and magnetic components are stacked up alternately until the bottom of the column is reached. Then the next column is taken (Fig. 2, right).

Each of these arrangements of the variables leads to a specific form of the matrix of the system of linear algebraic equations for the approximate field values. Arrangement (i) gives a four-block matrix which contains the principal mode coefficients in the diagonal blocks, and the coupling coefficients in the anti-diagonal blocks (Fig. 2 left). For isotropic structures the field modes, E and H, separate clearly into two matrices.

Arrangement (ii) mixes the principal mode coefficients and those arising due to inter-mode coupling together within each row, but leads to a more compact, band matrix (Fig. 2 right). Although we have not tried an exact proof, in our opinion this arrangement yields a matrix with the narrowest band possible. It may be easily shown that, after multiplying all the H-mode equations by a constant factor $i\omega\mu_0$, the matrix is symmetric (the same applies, naturally, also to matrix (i)). In our computer program we prefer arrangement (ii), as it allows Gaussian elimination, in a special modification for symmetric, band matrices, to be used to solve the FD linear algebraic system. To store the upper half-band of the matrix, as required by the modified algorithm of Gaussian elimination, needs N_{STOR} complex numbers to be placed in memory,

$$N_{STOR} = \underbrace{(N-1)(2M_E + M_A - 2)}_{number\ of\ equations}\ \underbrace{(2M_E + M_A + 1)}_{band-width},$$

where N is the number of horizontal grid steps, and M_E, M_A are the numbers of vertical grid steps within the conducting earth and in the air layer, respectively. This is usually by far the most memory consuming part of the modelling algorithm.

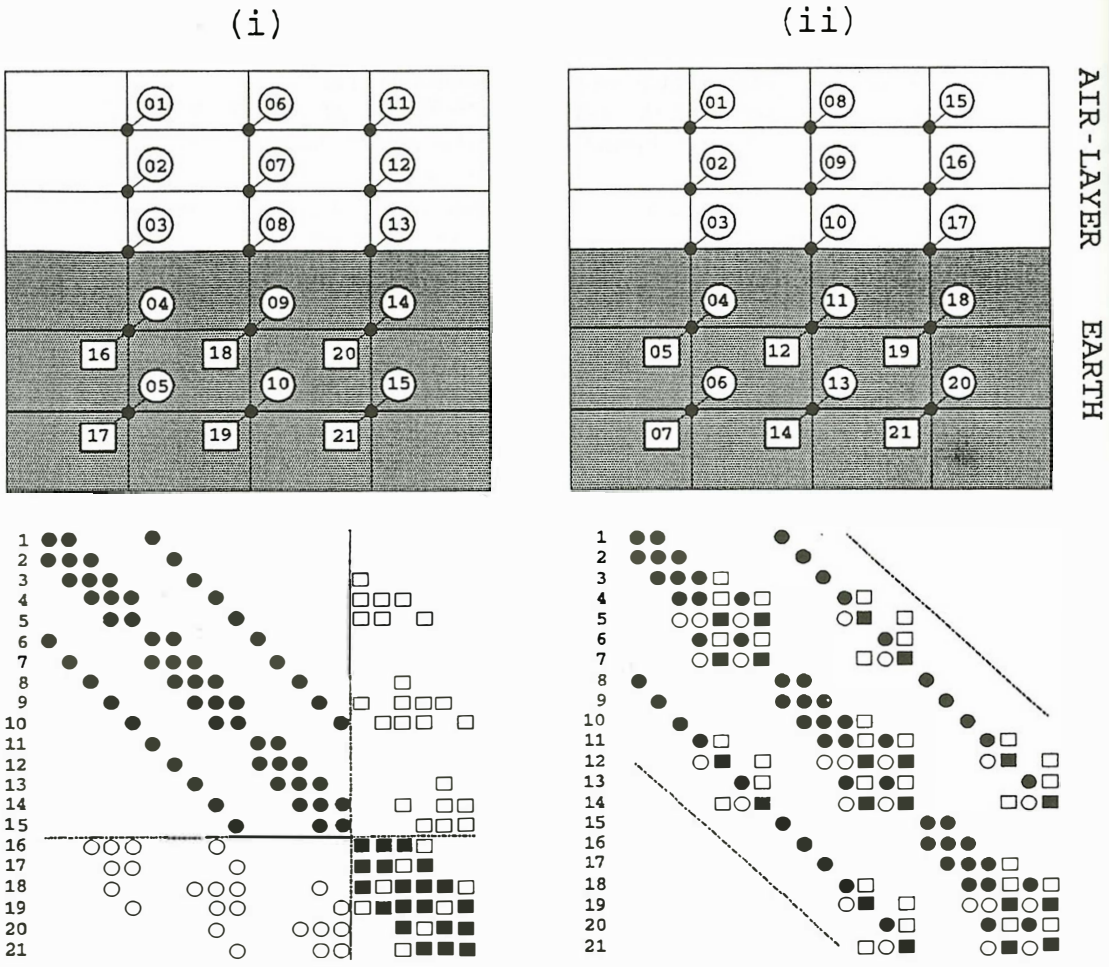

Figure 2: Two variants of ordering the variables throughout the grid, along with a symbolic form of the resulting matrices of the systems of FD equations. Circles are for electric components, squares for magnetic components, emtpy symbols in matrix patterns are for coefficients which arise only due to anisotropy.

5 Magnetotelluric functions on the earth's surface

Solving the system of linear FD equations provides us with approximate values of the field components E_x and H_x at all grid points. For practical purposes, all components of the magnetotelluric field must be evaluated on the earth-air interface. From these, various magnetotelluric functions and parameters can be computed as practice-oriented modelling outputs.

Knowing E_x and H_x throughout the grid, values of the 'secondary' field components E_y, E_z, H_y, and H_z can be evaluated at any grid point using equations (3), (4), and (6), (7)

$$E_y = \frac{\sigma_{yz}}{D}\frac{\partial H_x}{\partial y} + \frac{\sigma_{zz}}{D}\frac{\partial H_x}{\partial z} + K\,E_x, \qquad H_y = \frac{1}{i\omega\mu_0}\frac{\partial E_x}{\partial z},$$

$$E_z = -\frac{\sigma_{yy}}{D}\frac{\partial H_x}{\partial y} - \frac{\sigma_{zy}}{D}\frac{\partial H_x}{\partial z} + L\,E_x, \qquad H_z = -\frac{1}{i\omega\mu_0}\frac{\partial E_x}{\partial y}.$$

On the surface, $E_z = 0$ and $\partial H_x/\partial y = 0$, as no vertical current can flow through the earth-air interface. The remaining field components on the surface are computed by approximating numerically the derivatives $\partial E_x/\partial y$, $\partial E_x/\partial z$, and $\partial H_x/\partial z$ in above formulae. In our computer program a 3-point differences, based on parabolic interpolation, are used to approximate these derivatives. However, for a next version, we intend to employ refined formulae for the spatial derivatives, similar to those derived in [22, 23].

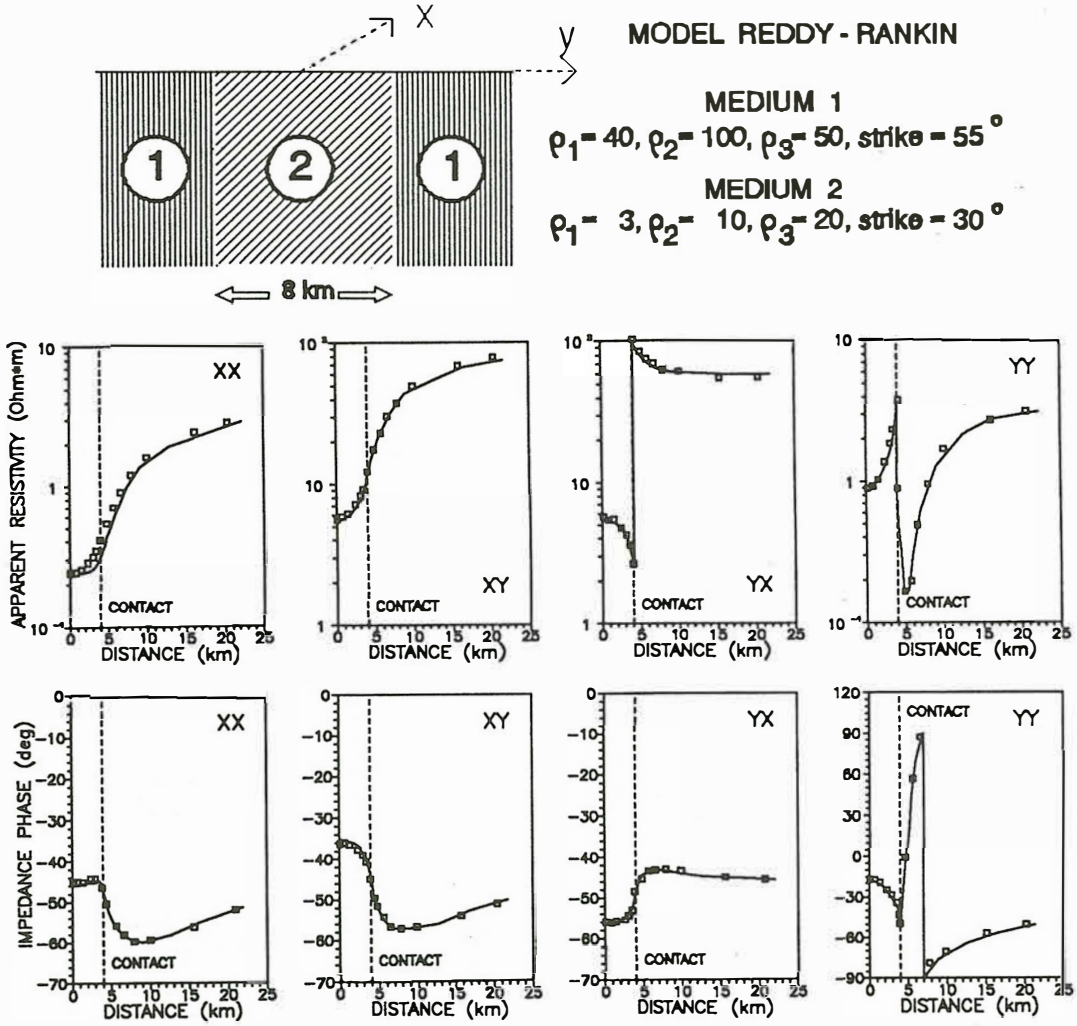

Figure 3: Comparison of apparent resistivities (upper row of plots) and phases (lower row of plots) for the horizontally anisotropic dyke model of Reddy and Rankin [10]. The comparison is carried out along a $25km$ section from the center of the model to the right. Dashed line at $4km$ indicates the position of the contact. Solid line—modelling results of Reddy and Rankin [10], squares—results obtained by the present FD algorithm.

The magnetotelluric and geomagnetic transfer functions on the earth's surface (impedances, admitances, components of the induction vectors, etc.) are evaluated using the field components computed for two independent polarizations of the primary electromagnetic wave. Anisotropy within a 2-D structure leads in general to a full and non-diagonizable impedance tensor, imitating thus locally a 3-D underground. Other magnetotelluric parameters, such as Swift's principal direction, skew, ellipticity, etc., can be now computed easily.

6 Numerical tests

There are only few chances to check the results of our modelling algorithm with other independent computations. Except some trivial checks, such as the identity of magnetotelluric functions when different polarizations of the primary wave are used, we carried out the following tests:

a) The results for an isotropic structure are identical with those obtained independently by a 2-D 'isotropic' modelling program of Červ and Praus [20] for the same model.

b) The results for a 1-D anisotropic layered structure, approximated as a 2-D model, are practically identical with those obtained independently by a 1-D algorithm based on the matrix propagation of the

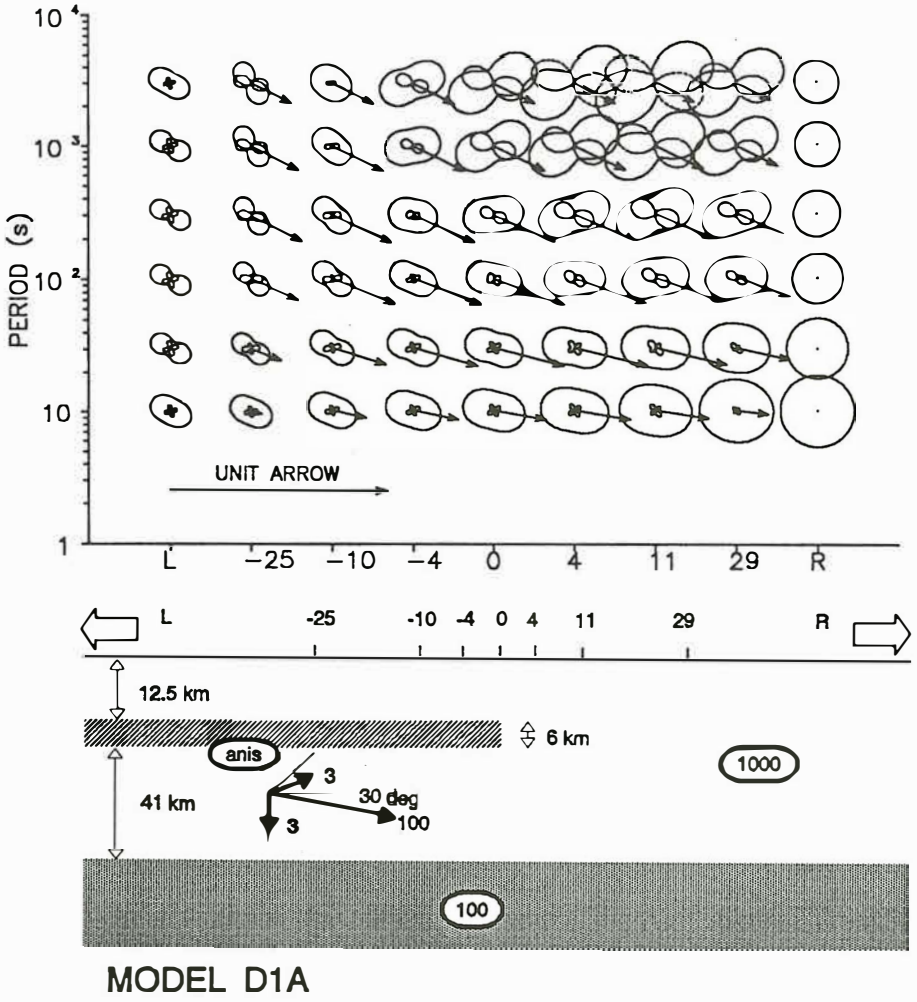

Figure 4: Real induction arrows and polar impedance diagrams for a two-layer earth with an anisotropic layer inserted in the first layer. The conductivity tensor of the anisotropic layer is given by the principal resistivities $\rho_x/\rho_y/\rho_z = 3/100/3$ and the anisotropy strike of 30 degrees towards R. All resistivities are in Ωm.

electromagnetic fields through the layers. The deviations do not exceed one percent, except inadequate grid parameters are chosen.

c) Reddy and Rankin [10] studied a 2-D horizontally anisotropic dyke model in detail. In Fig. 3 a comparison of our results with those taken from [10] is shown for a set of magnetotelluric functions—apparent resistivities and phases. For this model the results are almost identical, very small differences are observed only near the dyke contacts, where the difference in the approximation techniques is likely to play some role.

7 Numerical examples

We will demonstrate the developed algorithm by showing two simple models which illustrate the effect of strong electrical anisotropy upon magnetotelluric functions and induction arrows. We chose these models since absolutly nothing could have been said earlier about induction arrows in anisotropic structures with solely 1-D modelling algorithms available.

Model in Fig. 4 consists of a two layer earth with an anisotropic half-layer inserted in the first layer. The principal resistivities of the anisotropic inhomogeneity are $\rho_x/\rho_y/\rho_z = 3/100/3$, in Ωm, and the anisotropy strike is 30 degrees with respect to the structural strike of the model. In the upper part of

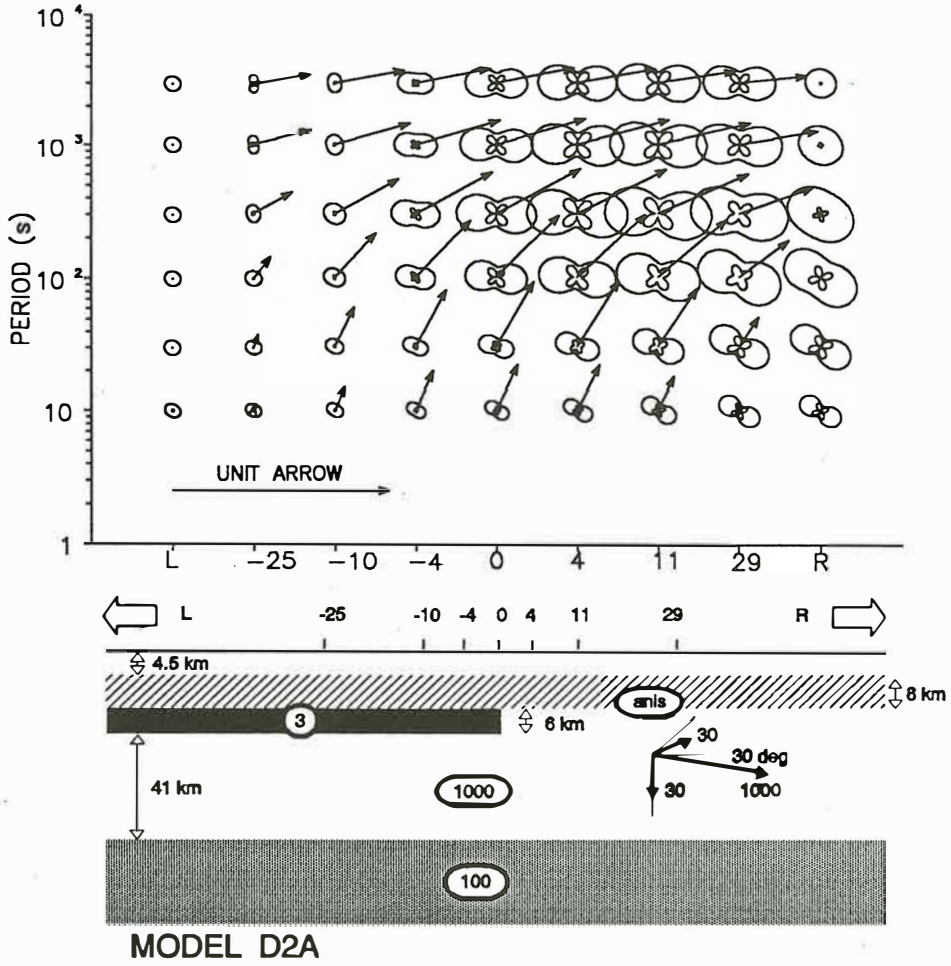

Figure 5: Real induction arrows and polar impedance diagrams for a model with a lateral conductivity contact overlaid with an anisotropic layer. The conductivity tensor of the anisotropic layer is given by the principal resistivities $\rho_x/\rho_y/\rho_z = 30/1000/30$ and the anisotropy strike of 30 degrees towards R. All resistivities are in Ωm.

Fig. 4 real induction arrows, along with polar impadance diagrams for Z_{xx} and Z_{xy}, are shown for selected points along the model's surface and for a series of periods from 10 to 3000s. Under the influence of the anisotropic half-layer, real induction arrows behave as qualitatively expected—they are deflected so as to keep their perpendicular direction with respect to the predominant induced currents. Similar effect can be observed for the polar impedance diagrams Z_{xy}—their minimum axes indicate the direction of preferred conductivity, i.e. the anisotropy strike in this case. For long periods, however, and also for increasing distance from the contact into the isotropic quarter-space, the fade-away of the anisotropy contact effect is connected with certain over-relaxation expressed by a contrary orientation of the impedance diagrams.

Different pattern, however, is observed if two isotropic domains make contact and the effect of an additional anisotropic layer is superimposed over that excited by the lateral inhomogeneity. Model in Fig. 5 is a modified version of the preceding model—the conducting half-layer is made isotropic and it is overlaid with an additional anisotropic layer. In this case, the real induction arrows are orientated *in the direction of preferred conductivity of the anisotropic layer*, and not perpendicularly to it as one would expect. We explain this phenomenon by the effect of compensation currents within the anisotropic layer, which try to cancel out the vertical magnetic field excited by the underlying lateral conductivity contrast. In an isotropic structure, these compensating currents would be of opposite direction with respect to the exciting currents and would cause the induction arrows on the surface to become smaller.

With anisotropy within the layer, the compensating currents are deflected, and the resulting induction arrows are rotated *towards* the direction of preferred conductivity. The impedance diagrams for this model behave as intuitively expected, their minimum axes are turned into the direction of preferred conductivity. Quite a similar effect as that described here for an anisotropic cover is observed if the anisotropic layer is situated below the lateral contact, only the frequency range of the maximum anisotropy influence is shifted, towards longer periods, due to a greater depth of the layer.

We consider the results of these simple modellings quite interesting as regards the induction studies in a regional vicinity of the KTB borehole. A discrepancy often discussed when considering induction data from this area consists in a regionally observed directional difference of induction arrows and principal impedances—while the impedances display rather strong anisotropy with minimum axes directed predominantly towards NW, the induction vectors are almost uniformly directed towards S, for longer periods from 10 *s* at least. Without penetrating deeper into this problem, we only want to emphasize that within the class of 2-D anisotropic models such a relation between impedances and induction arrows is quite possible.

References

[1] Tezkan, B., 1988. Ein Interpretationsversuch zur Erklärung der konträren Phasenverlaufe der E- und B-Polarisation am Ostrand der Hessischen Senke mit zweidimensionalen Leitfähigkeitsmodellen, in *Protokoll Kolloquium Elektromagnetische Tiefensondierung, Königstein, 1-3 March 1988,* pp. 35–54. eds Haak, V. & Homilius, J., Niedersächsisches Landesamt für Bodenforschung, Hannover.

[2] Tezkan, B., Červ, V. & Pek, J., 1992. Resolution of anisotropic and shielded highly conductive layers using 2-D electromagnetic modelling in the Rhine Graben and Black Forest, *Phys. Earth planet. Inter.,* **74,** 159–172.

[3] Eisel M., 1994. Modell Oberpfalz-anisotrop. Paper presented at *Kolloquium Elektromagnetische Tiefenforschung, Höchst/Odenwald, 29-31 March 1994.*

[4] Tauber, S., 1993. Die Leitfähigkeitsverteilung in den nördlichen Varisziden untersucht mit den Methoden der Magnetotellurik und der geomagnetischen Tiefensondierung auf einem Profil vom Oberpfälzer Wald ins Vogtland. *Diploma thesis,* Inst. für Geol., Geoph. und Geoinform., Freie Universität Berlin, 102 pp.

[5] Červ, V., Pek, J. & Praus O., 1993. MT and MV measurements in SW Bohemia. In *KTB-Report,* (submitted).

[6] Eisel, M., 1992. Effekte lateral anisotroper Leitfähigkeitsstrukturen in der MT, in *Protokoll Kolloquium Elektromagnetische Tiefenforschung, Borkheide, 25-29 Mai 1992,* eds Haak, V. & Rodemann, H., Deutsche Geophysikalische Gesellschaft.

[7] Eisel, M. & Bahr, K., 1993. Electrical anisotropy in the lower crust of British Columbia: an interpretation of a magnetotelluric profile after tensor decomposition, *J. Geomag. Geoelectr.,* **45,**1115–1126.

[8] Jones, A. G., Groom, R. W. & Kurtz, R. D., 1993. Decomposition and modelling of the BC87 dataset, *J. Geomag. Geoelectr.,* **45,** 1127–1150.

[9] Rasmussen, T. M., 1988. Magnetotellurics in southwestern Sweden: evidence for electrical anisotropy in the lower crust?, *J. Geophys. Res.,* **93,** 7897–7907.

[10] Reddy, I. K. & Rankin, D., 1975. Magnetotelluric response of laterally inhomogeneous and anisotropic structure, *Geophysics,* **40,** 1035–1045.

[11] Saraf, P. D., Negi, J. G. & Červ, V., 1986. Magnetotelluric response of a laterally inhomogeneous anisotropic inclusion, *Phys. Earth planet. Inter.,* **43,** 196–198.

[12] Xiong, Z., 1989. Electromagnetic fields of electric dipoles embedded in a stratified anisotropic earth, *Geophysics,* **54,** 1643–1646.

[13] Osella, A. M. & Martinelli, P., 1993. Magnetotelluric response of anisotropic 2-D structures, *Geophys. J. Int. ,* **115,** 819–828.

[14] Schmucker, U., 1994. 2 dimensionale dünne Schichten über anisotropen geschichteten Halbräumen, Poster presented at *Kolloquium Elektromagnetische Tiefenforschung, Höchst/Odenwald, 29–31 March 1994.*

[15] Grubert, D., 1994. Eine Verallgemeinerung der klassischen Lösung von d'Erceville & Kunetz für anisotrope Widerstände, Poster presented at *Kolloquium Elektromagnetische Tiefenforschung, Höchst/Odenwald, 29–31 March 1994.*

[16] Reddy, I. K., & Rankin, D., 1971. Magnetotelluric effect of dipping anisotropies, *Geophys. Prosp.,* **19,** 84-97.

[17] Loewenthal, D. & Landisman, M., 1973. Theory for magnetotelluric observations on the surface of a layered anisotropic half space, *Geophys. J. R. astr. Soc.,* **35,** 195–214.

[18] Brewit-Taylor, C. R. & Weaver, J. T., 1976. On the finite difference solution of two-dimensional induction problems, *Geophys. J. R. astr. Soc.,* **47,** 375–396.

[19] Haak, V., 1972. Magnetotellurik: Bestimmung der Übertragungsfunktionen in Gebieten mit lateraler Änderung der elektrischen Leitfähigkeit, *Z. Geophys.,* **38,** 85–102.

[20] Červ, V. & Praus, O., 1978. Numerical modelling in laterally inhomogeneous geoelectrical structures. *Studia Geophys. et Geodaet.,* **22,** 72–81.

[21] Yudin, M. N., 1982. Algorithm of selection of net parameters in calculations of magnetotelluric field by the finite-difference method, in *Geomagnetic Researches No. 29,* pp. 91–95, eds Vanyan, L. L., Debabov, A. S. & Kharin, J. P., Radio i Svyaz, Moscow (in Russian).

[22] Weaver, J. T., Le Quang, B. V. & Fischer, G., 1985. A comparison of analytical and numerical results for a two dimensional control model in electromagnetic induction. I. B-polarization calculations, *Geophys. J. R. astr. Soc.,* **82**(2) , 263–277.

[23] Weaver, J. T., Le Quang, B. V. & Fischer, G., 1986. A comparison of analytical and numerical results for a two dimensional control model in electromagnetic induction. I. E-polarization calculations, *Geophys. J. R. astr. Soc.,* **87,** 917–948.

Appendix

FD schemes and coefficients

FD scheme and coefficients C^{EE}_{jk} (top half-box) and C^{EH}_{jk} (bottom half-box) for the E-mode at the grid node (j,k)

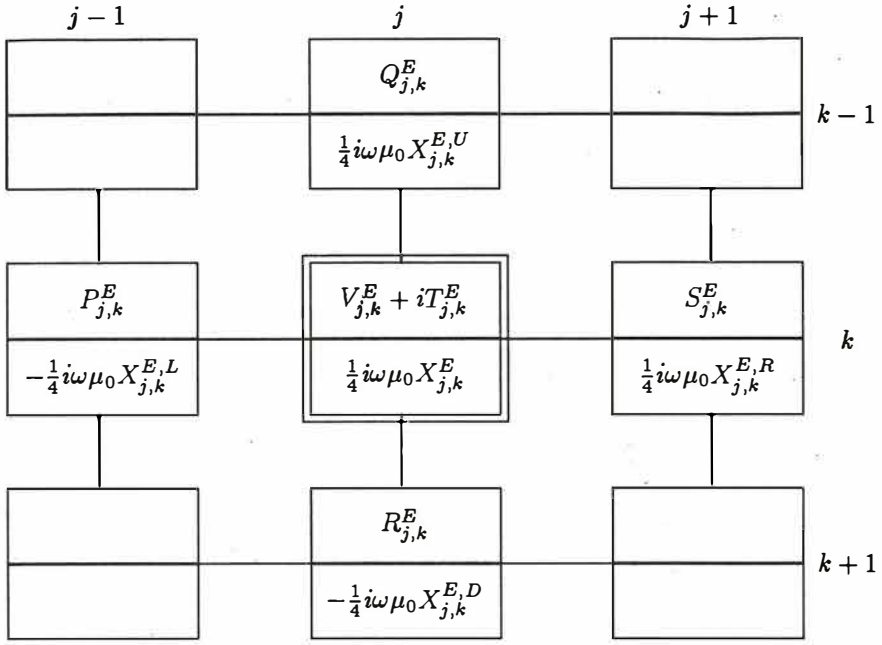

$$P^E_{j,k} = (h^{(z)}_k + h^{(z)}_{k+1})/(2h^{(y)}_j), \qquad Q^E_{j,k} = (h^{(y)}_j + h^{(y)}_{j+1})/(2h^{(z)}_k),$$

$$R^E_{j,k} = (h^{(y)}_j + h^{(y)}_{j+1})/(2h^{(z)}_{k+1}), \qquad S^E_{j,k} = (h^{(z)}_k + h^{(z)}_{k+1})/(2h^{(y)}_{j+1}),$$

$$V^E_{j,k} = -(P^E_{j,k} + Q^E_{j,k} + R^E_{j,k} + S^E_{j,k}),$$

$$T^E_{j,k} = \frac{1}{4}\omega\mu_0 \sum_{p=j}^{j+1}\sum_{q=k}^{k+1} (\sigma_{xx} + A\sigma_{zx} + B\sigma_{yx})_{p,q}\, h^{(y)}_p h^{(z)}_q$$

$$X^{E,L}_{j,k} = h^{(z)}_k A_{j,k} + h^{(z)}_{k+1} A_{j,k+1}, \qquad X^{E,R}_{j,k} = h^{(z)}_k A_{j+1,k} + h^{(z)}_{k+1} A_{j+1,k+1},$$

$$X^{E,U}_{j,k} = h^{(y)}_j B_{j,k} + h^{(y)}_{j+1} B_{j+1,k}, \qquad X^{E,D}_{j,k} = h^{(y)}_j B_{j,k+1} + h^{(y)}_{j+1} B_{j+1,k+1},$$

$$X^E_{j,k} = X^{E,L}_{j,k} - X^{E,U}_{j,k} + X^{E,D}_{j,k} - X^{E,R}_{j,k}.$$

FD scheme and coefficients C_{jk}^{HE} (top half-box) and C_{jk}^{HH} (bottom half-box) for the H-mode at the grid node (j,k)

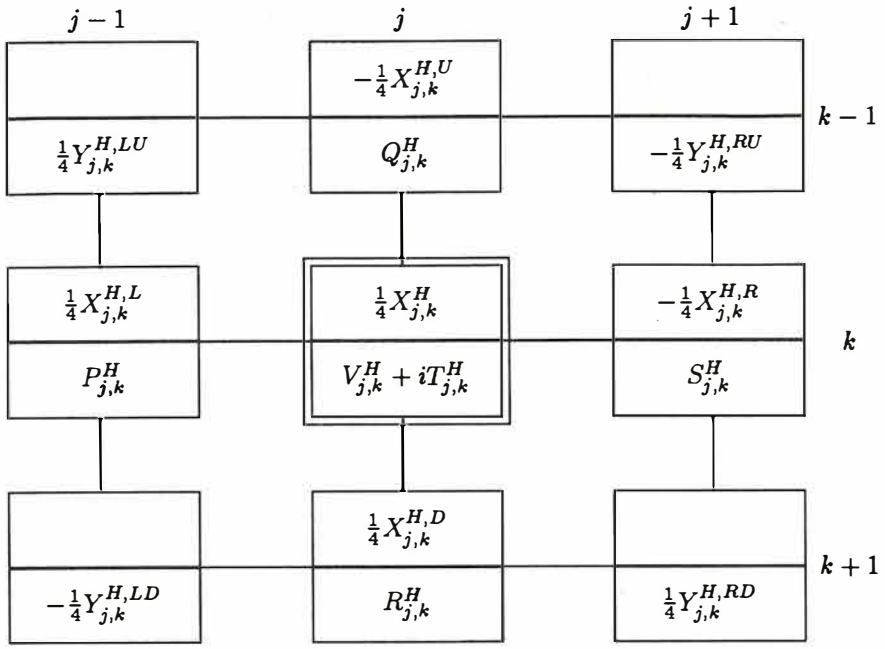

$$P_{j,k}^{H}=[h_k^{(z)}\,(\sigma_{yy}/D)_{j,k}+h_{k+1}^{(z)}\,(\sigma_{yy}/D)_{j,k+1}]/(2h_j^{(y)}),$$

$$Q_{j,k}^{H}=[h_j^{(y)}\,(\sigma_{zz}/D)_{j,k}+h_{j+1}^{(y)}\,(\sigma_{zz}/D)_{j+1,k}]/(2h_k^{(z)}),$$

$$R_{j,k}^{H}=[h_j^{(y)}\,(\sigma_{zz}/D)_{j,k+1}+h_{j+1}^{(y)}\,(\sigma_{zz}/D)_{j+1,k+1}]/(2h_{k+1}^{(z)}),$$

$$S_{j,k}^{H}=[h_k^{(z)}\,(\sigma_{yy}/D)_{j+1,k}+h_{k+1}^{(z)}\,(\sigma_{yy}/D)_{j+1,k+1}]/(2h_{j+1}^{(y)}),$$

$$V_{j,k}^{H}=-(P_{j,k}^{H}+Q_{j,k}^{H}+R_{j,k}^{H}+S_{j,k}^{H})-\frac{1}{4}(Y_{j,k}^{H,LU}-Y_{j,k}^{H,RU}+Y_{j,k}^{H,LD}-Y_{j,k}^{H,RD}),$$

$$T_{j,k}^{H}=\frac{1}{4}\omega\mu_0(h_j^{(y)}+h_{j+1}^{(y)})(h_k^{(z)}+h_{k+1}^{(z)}),$$

$$X_{j,k}^{H,L}=h_k^{(z)}L_{j,k}+h_{k+1}^{(z)}L_{j,k+1},\quad X_{j,k}^{H,R}=h_k^{(z)}L_{j+1,k}+h_{k+1}^{(z)}L_{j+1,k+1},$$

$$X_{j,k}^{H,U}=h_j^{(y)}K_{j,k}+h_{j+1}^{(y)}K_{j+1,k},\quad X_{j,k}^{H,D}=h_j^{(y)}K_{j,k+1}+h_{j+1}^{(y)}K_{j+1,k+1},$$

$$X_{j,k}^{H}=X_{j,k}^{H,L}-X_{j,k}^{H,U}+X_{j,k}^{H,D}-X_{j,k}^{H,R},$$

$$Y_{j,k}^{H,LU}=(\sigma_{zy}/D)_{j,k}+(\sigma_{yz}/D)_{j,k},\ Y_{j,k}^{H,RU}=(\sigma_{zy}/D)_{j+1,k}+(\sigma_{yz}/D)_{j+1,k},$$

$$Y_{j,k}^{H,LD}=(\sigma_{zy}/D)_{j,k+1}+(\sigma_{yz}/D)_{j,k+1},\ Y_{j,k}^{H,RD}=(\sigma_{zy}/D)_{j+1,k+1}+(\sigma_{yz}/D)_{j+1,k+1}.$$